A new analytical model for transient heat transfer modeling of geothermal monotube heat exchangers

Yves Jannot, Anas El Maakoul, Christian Moyne, Alain Degiovanni

A new analytical model for transient heat transfer modeling of geothermal monotube heat exchangers

Yves Jannot [a], Anas El Maakoul [b*] , Christian Moyne [a], Alain Degiovanni [a,b]

[a] Université de Lorraine, CNRS, LEMTA, F-54500 Vandoeuvre les Nancy, France.

[b] International University of Rabat, LERMA Lab, 11000 Sala Al Jadida, Morocco

Corresponding author: Anas El Maakoul, International University of Rabat, LERMA Lab, 11000 Sala Al Jadida, Morocco, e-mail: anas.elmaakoul@uir.ac.ma

Abstract:

In this study, we present a new analytical model for the analysis of transient heat transfer (the model is solved after Laplace transformation) in geothermal monotube heat exchangers (GHE). The model accounts for various factors, including the heat exchanger's geometric parameters, the nature of the fluid (air and water), flow characteristics (laminar and turbulent), and heat transfer boundary conditions. Initially, the model's performance is validated by comparing its results with those obtained from computational fluid dynamics simulations using OpenFOAM. This validation process ensures the reliability and accuracy of the model. Additionally, an analysis of the heat transfer mechanisms and key modeling parameters identified from the comparison is provided. In the subsequent section, the analysis is extended by comparing the proposed model to four existing analytical models available in the literature. These reference models employ distinct approaches to simulate heat transfer to the ground. By examining a range of cases, the performance of the model is systematically evaluated against these conventional methods. This work closes by an analysis of the analytical models and the impact on the accuracy of the results highlighting the advantages of the proposed method in geothermal applications.

Nomenclature

a_s	Soil thermal diffusivity ($m^2\ s^{-1}$)
c_f	Fluid specific heat ($J\ kg^{-1}\ K^{-1}$)
h	Convective heat transfer coefficient ($W\ m^{-2}\ K^{-1}$)
L	Tube length (m)
$\dot{m}_f$	Fluid mass flow rate ($kg\ s^{-1}$)
p	Laplace parameter (s^{-1})
P	Pressure (Pa)
r	Space variable (m)
r_i	Inner radius of the tube (m)
r_e	Outer radius of the tube (m)
t	Time variable (t)
T_f	Fluid temperature (K)
T_i	Initial soil temperature (K)
T_s	Soil temperature (K)
T_t	Tube temperature (K)
v_f	Fluid velocity ($m\ s^{-1}$)
z	Space variable (m)
λ_f	Fluid Thermal conductivity ($W\ m^{-1}\ K^{-1}$)
λ_s	Soil Thermal conductivity ($W\ m^{-1}\ K^{-1}$)
λ_t	Tube Thermal conductivity ($W\ m^{-1}\ K^{-1}$)
ρ_f	Fluid density ($kg\ m^{-3}$)
θ_s	Laplace transform of the soil temperature ($K\ s$)

θ_f Laplace transform of the fluid temperature ($K\ s$)

1. Introduction

The increasing emphasis on sustainable heating and cooling solutions has propelled geothermal energy into the forefront of efforts to electrify and decarbonize the space heating and cooling sector [1]. Geothermal Heat Exchangers (GHEs) harness the potential of shallow geothermal reserves by utilizing embedded ground heat exchangers, offering both economic and environmental benefits. Essentially, a GHE comprises a conduit within a vertical or horizontal borehole through which a heat-carrying fluid circulates, enabling heat absorption in winter and discharge in summer [2]. The intricate heat exchange phenomena, coupled with the distinctive ground properties and flow dynamics, present both opportunities and challenges. Understanding the thermal processes in the ground is crucial for optimizing strategies in energy systems that integrate GHEs. Experimentation is generally impractical due to the large scale of GHEs and their thermal coupling to the ground, where geometric configurations and location-specific soil properties significantly influence performance. For engineers and researchers alike, the value of any design solutions lies in their applicability in the design of heat transfer equipment in a practical manner with reasonable accuracy. Consequently, theoretical predictions from heat-transfer models emerge as the most practical and cost-efficient approach to developing these strategies [3].

Theoretical analyses rely on heat transfer and fluid flow considerations, employing both analytical and numerical methods. These methods vary in terms of accuracy, complexity, and computation time. Their primary goal is to predict the returning fluid temperature and ground temperature near the heat exchanger [4, 5]. Additionally, they serve as tools for inverse parameter estimation, such as thermal response tests, for estimating critical parameters like soil thermal conductivity and diffusivity [6, 7]. Many analytical models are rooted in Kelvin's theory of heat sources and the Laplace transform method, as extensively described in the classic work of Carslaw and Jaeger [8]. These models, including the infinite cylindrical-surface source model [9], infinite line-source model [9], finite line-source model [10], and composite-medium line-source model [11], can be incorporated into building simulation tools due to their computational efficiency and, in specific cases, acceptable accuracy. A comprehensive comparison of these conventional models, considering temporal and spatial scales, can be found in [2]. The infinite line-source model and its derivatives are widely adopted in GHE simulations for their simplicity and relatively good accuracy [12-14].

Numerical models, on the other hand, can be based on finite-difference, finite-volume, and finite-element methods [15-20]. While these methods offer detailed insights into thermal, fluid flow, and pressure fields, they are often impractical for engineering applications for several reasons [2, 21]. They demand extensive computational resources and require important computation time, particularly in complex scenarios where all time and space scales are significant. Developing a versatile in-house code is challenging as these codes may have limitations in handling a wide array of GHE configurations, particularly when rapid prototyping and extensive model variations are necessary. Moreover, integrating such software into existing building simulation tools (e.g., EnergyPlus) can be cumbersome. Commercial software packages like ANSYS and COMSOL, often used for numerical simulations, may not be readily adaptable to specific applications. Consequently, many researchers advocate for general design and simulation tools grounded in analytical heat-transfer models for GHE modeling. For these reasons, numerical simulations in this work, utilizing open-source codes, are used to validate and compare with our proposed analytical model. A comprehensive review of analytical and numerical methods used for GHE can be found in recent literature [1, 2, 22].

This paper proposes an analytical model based on the quadruple formalism (Laplace transform) for transient heat transfer modeling in geothermal monotube heat exchangers. Traditionally, analytical models using the Laplace transform faced challenges due to the computational complexity of conducting the inverse Laplace transform. However, recent advancements in mathematical algorithms

and computational capabilities, as demonstrated in this work, have substantially mitigated this limitation. The primary objectives of our study are to achieve heightened precision compared to conventional analytical models while maintaining rapid computational efficiency, as opposed to numerical methods. We explore various configurations, accounting for diverse geometrical parameters, fluid types (air and water), flow regimes (laminar and turbulent), and thermal conditions. Our approach begins with a detailed mathematical description of the model and its underlying assumptions, followed by a comparison with numerical results obtained using computational fluid dynamics codes with OpenFOAM. Additionally, we compare the proposed model to four existing analytical models from the literature, including the commonly employed infinite line-source model, under similar conditions. One of the main advantages of the proposed model is its accurate use of the convolution product, which improves the accuracy of calculations, particularly when the exchanger inlet temperature is variable. Our model increases the reliability of forecasts in transient heat transfer scenarios.

2. System and mathematical model

2.1. Description

The geothermal heat exchanger under consideration is a tube buried under ground at a depth D_s from the ground surface. A fluid flows inside the tube with an inlet velocity $v_{f,in}$, inlet temperature $T_f(0)$ and outlet temperature $T_f(L)$. The tube has a length L, inner radius r_i and outer radius $r_e = r_i + e$. The ground is assumed to be an infinite medium (D_s sufficiently large).

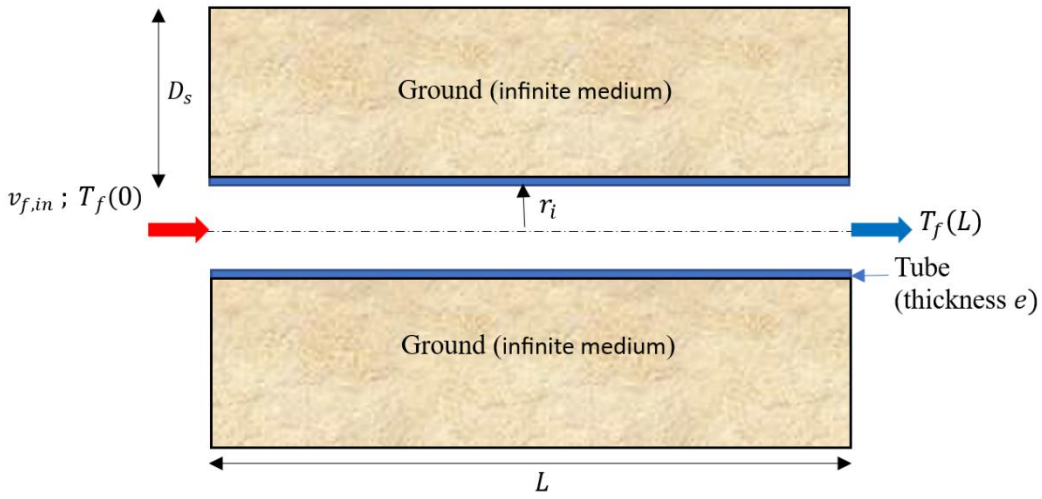

Figure 1. Schematic of the modeled system

2.2. Proposed analytical model

The analytical model is based on the heat equation with the following assumptions:

- Ground temperature variations in time and space are very small, so the temperature far away from the pipe will be considered constant throughout the problem.
- In soil, the axial temperature gradient is negligible compared to the radial gradient.
- The mass of the tube is neglected.
- Thermophysical properties of the soil, tube and fluid are assumed homogeneous and constant.
- The fluid velocity is assumed to be constant along the length of the tube.

These assumptions are inherent in the approach of many analytical methods, including ours, and will be justified through validation by comparing our model against comprehensive numerical simulations conducted without the numerous assumptions commonly found in analytical models.

The heat equation applied to the soil is:

$$\frac{1}{a_s}\frac{\partial T_s}{\partial t} = \frac{1}{r}\frac{\partial}{\partial r}\left(r\frac{\partial T_s}{\partial r}\right) + \frac{\partial^2 T_s}{\partial z^2} \quad (1)$$

Neglecting the axial gradient:

$$\frac{1}{a_s}\frac{\partial T_s}{\partial t} = \frac{1}{r}\frac{\partial}{\partial r}\left(r\frac{\partial T_s}{\partial r}\right) \quad (2)$$

With the initial condition:

$$T_s(r, z, t = 0) = T_i \quad (3)$$

And boundary conditions:

$$T_s(r \to \infty, z, t) = T_i \quad (4)$$

$$\lambda_s \frac{\partial T_s}{\partial r}(r = r_e)2\pi r_e = \frac{T_t(r_i) - T_f}{R_f} = \frac{T_t(r_e) - T_t(r_i)}{R_t} = \frac{T_t(r_e) - T_f}{R_f + R_t} \quad (5)$$

$$T_t(r_e) = T_s(r_e) \quad (6)$$

and therefore:

$$\lambda_s \frac{\partial T_s}{\partial r}(r = r_e) = h_g\left[T_s(r_e) - T_f\right] \quad (7)$$

Where:

$$h_g = \frac{1}{2\pi r_e} \times \frac{1}{R_f + R_t} \quad (8)$$

$R_f = \frac{1}{2\pi r_i h}$ (thermal resistance of the fluid) (9)

$R_t = \frac{\ln\left(\frac{r_e}{r_i}\right)}{2\pi\lambda_t}$ (thermal resistance of the tube) (10)

With:

T_i initial temperature of the soil
λ_s soil thermal conductivity
h convective heat transfer coefficient
λ_t tube thermal conductivity.

The Laplace transformation applied to equation (1) with the Laplace transformed soil temperature $\theta_s(r, z, p) = \mathcal{L}[T_s(r, z, t) - T_i]$ leads to:

$$p\,\frac{\theta_s}{a_s} = \frac{1}{r}\frac{\partial}{\partial r}\left(r\frac{\partial \theta_s}{\partial r}\right) \quad (11)$$

The solution is of the form:

$$\theta_s(r, z, p) = A\, I_0(qr) + B\, K_0(qr) \quad (12)$$

Where $q = \sqrt{\frac{p}{a_s}}$ and I_0 and K_0 are the zero order modified Bessel functions of first and second kind respectively.

Using the boundary condition (4):

$$\theta_s(r \to \infty, z, t) = 0 \quad (13)$$

Therefore $A = 0$, and using the boundary condition (7):

$$-\lambda_s\, qB\, K_1(qr_e) = h_g\theta_s(r_e) - h_g\,\theta_f = h_g\, B\, K_0(qr_e) - h_g\,\theta_f \tag{14}$$

we obtain: $B = \frac{\theta_f}{K_0(qr_e)+\frac{\lambda_s q}{h_g}K_1(qr_e)}$ (15)

with θ_f the Laplace transform of fluid temperature.

Equation (12) can then be written as:

$$\theta_s(r,z,p) = \frac{K_0(qr)}{K_0(qr_e)+\frac{qr_e}{Bi}K_1(qr_e)}\;\theta_f(z,p) \tag{16}$$

Where: $Bi = \frac{h_g r_e}{\lambda_s}$ (17)

The soil model can then be coupled with the fluid heat balance between z and $z + dz$ in the tube's axial direction, which is written as:

$$2\pi r_e\lambda_s dz\,\frac{\partial T_s}{\partial r}(r = r_e) = \rho_f c_f v_f\,\pi {r_i}^2\,\left[T_f(z+dz) - T_f(z)\right] \tag{18}$$

Where $\rho_f, c_f,$ and v_f are respectively the fluid density, specific heat, and velocity. Relation (18) can also be written as:

$$2\lambda_s\, r_e\,\frac{\partial T_s}{\partial r}(r = r_e) = \rho_f c_f v_f\, {r_i}^2\,\frac{\partial T_f}{\partial z} \tag{19}$$

The Laplace transformation of this equation, with $\theta_f = \mathcal{L}\left[\overline{T}_f(z,t)\right]$ and $\overline{T}_f(z,t) = T_f(z,t) - T_i$, leads to:

$$2\lambda_s r_e\,\frac{\partial\theta_s}{\partial r}(r = r_e) = \rho_f c_f v_f\, {r_i}^2\,\frac{\partial\theta_f}{\partial z} \tag{20}$$

Using equation (16) and solving equation (20) leads to:

$$\frac{\partial\theta_f}{\partial z} = \frac{2\lambda_s r_e}{\rho_f c_f\, v_f\, {r_i}^2}\,\frac{\partial\theta_s}{\partial r}(r = r_e) = -\frac{2\lambda_s q r_e}{\rho_f c_f\, v_f\, {r_i}^2}\,\frac{K_1(qr_e)}{K_0(qr_e)+\frac{qr_e}{Bi}\,K_1(qr_e)}\;\theta_f \tag{21}$$

We obtain the Laplace transformed fluid temperature θ_f:

$$\theta_f(z,p) = \theta_f(0,p)\; exp\left[-\frac{2\lambda_s\, qr_e}{\rho_f c_f\, v_f\, r_i}\;\frac{K_1(qr_e)}{K_0(qr_e)+\frac{qr_e}{Bi}\,K_1(qr_e)}\;\frac{z}{r_i}\right] \tag{22}$$

And the Laplace transform of the soil temperature $\theta(r,z,p)$:

$$\theta_s(r,z,p) = \theta_f(0,p)\,\frac{K_0(qr)}{K_0(qr_e)+\frac{qr_e}{Bi}\,q\,K_1(qr_e)}\,exp\left[-\frac{2\lambda_s\, qr_e}{\rho_f c_f\, v_f\, r_i}\;\frac{K_1(qr_e)}{K_0(qr_e)+\frac{qr_e}{Bi}\,K_1(qr_e)}\;\frac{z}{r_i}\right] \tag{23}$$

If the fluid inlet temperature is constant $T_f(z=0) = T_{f0}$, then using (22) we obtain:

$$\overline{T}_f(z,t) = \mathcal{L}^{-1}\left\{\frac{T_{f0}-T_i}{p}\; exp\left[-\frac{2\lambda_s\, qr_e}{\rho_f c_f\, v_f\, r_i}\;\frac{K_1(qr_e)}{K_0(qr_e)+\frac{qr_e}{Bi}\,K_1(qr_e)}\;\frac{z}{r_i}\right]\right\} \tag{24}$$

However, if the fluid inlet temperature is not constant:

$$\overline{T}_f(z,t) = \overline{T}_f(0,t) \otimes \mathcal{L}^{-1}\{H(z,p)\} \tag{25}$$

Where:

$$H(z,p) = exp\left[-A\sqrt{p}\,\frac{K_1(C\sqrt{p})}{K_0(C\sqrt{p})+B\sqrt{p}\,K_1(C\sqrt{p})}\right] \quad (26)$$

$$A = \frac{2\lambda_s\, r_e\, z}{\rho_f c_f\, v_f\, \sqrt{a_s} {r_i}^2} \quad (27)$$

$$B = \frac{r_e}{\sqrt{a_s}\, Bi} \quad (28)$$

$$C = \frac{r_e}{\sqrt{a_s}} \quad (29)$$

In this case, calculating the convolution product is not a problem unless the limit, when $t \to 0^+$ for one of the two terms, is infinite. This is the case here because when $t \to 0^+$, $p \to \infty$ and $H(p) \to exp\left(-\frac{A}{B}\right)$ thus $\mathcal{L}^{-1}\{H(z,p)\} \to \infty$.

If this is caused by a Dirac at $t = 0$ (which is the case here) we can get around this numerical problem by calculating the inverse Laplace transform of the transfer function integral, i.e., $\frac{H(z,p)}{p}$ which tends towards $exp\left(-\frac{A}{B}\right)$ when $p \to \infty$. Applying the preceding to (22), we obtain:

$$\bar{T}_f(z,t) = \frac{d}{dt}\left\{\bar{T}_f(0,t) \otimes \mathcal{L}^{-1}\left[\frac{H(z,p)}{p}\right]\right\} \quad (30)$$

Equations (24) and (30) are used to calculate the fluid temperature at the outlet of the geothermal heat exchanger. A MATLAB program was developed to evaluate the inverse Laplace transform of the transfer function (DenIseger [23]) before carrying out the convolution product.

3. Validation

In this section, the proposed analytical model performance is validated by comparing its results with those obtained from numerical simulations codes developed based on OpenFOAM.

3.1. Cases

The system under consideration is a geothermal heat exchanger buried below the ground surface, consisting of a circular tube where the working fluid (air or water) flows inside, surrounded by a soil layer (cf. Figure 2). The geometric parameters for each fluid are listed in Table 1.

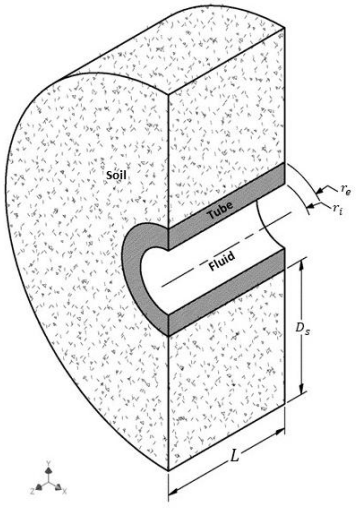

Figure 2. Schematic representation of the physical model (not to scale)

Table 1: Geometrical parameters		
Parameter	Air	Water

Inner tube radius $r_i\ (m)$	0.05	0.01
Outer tube radius $r_e\ (m)$	0.052	0.012
Soil distance $D_s\ (m)$	5	5
Length $L\ (m)$	20	30

Table 2 presents the ten considered validation cases. These cases consider two fluid types (air and water), two tube materials (PVC and steel), different flow regimes and different inlet temperature boundary conditions where:

- Initial soil temperature: $T_i = 0°C$
- Constant temperature boundary condition: $T_f(0) = 20°C$
- Periodic temperature boundary condition: $T_f(0,t) = T_{f0}\cos(\omega t)$ with $T_{f0} = 20°C$; $\omega = \frac{2\pi}{24\times3600}$ (one day period)

Table 2. Analytical and numerical comparisons cases ('x' represents Yes)

Case Nr	Inlet Temperature $T_f(z=0)$		Fluid type		Tube material		Flow inlet velocity v_f		
	Constant	Periodic	Air	Water	PVC	Steel	$2.829\ m\ s^{-1}$ (Turbulent)	$0.1\ m\ s^{-1}$ (Laminar)	$1\ m\ s^{-1}$ (Turbulent)
1	x		x		x		x		
2	x		x			x	x		
3	x			x	x			x	
4	x			x	x				x
5	x			x		x		x	
6	x			x		x			x
7		x	x		x		x		
8		x	x			x	x		
9		x		x	x			x	
10		x		x		x		x	

The thermo-physical properties for the various materials and fluids are given in Table 3.

Table 3. Thermo-physical properties

Matter	λ (W m^{-1} K^{-1})	ρ (kg m^{-3})	c (J kg^{-1} K^{-1})	μ (Pa s)
Air	0.025	1.2	1006	1.8×10^{-5}
Water	0.6	1000	4180	10^{-3}
PVC	0.2	1459	1034	
Steel	15	7864	460	
Soil	1.9	1500	1269	

3.2. Numerical simulations

In this section, we present the numerical simulations performed to investigate the dynamic heat transfer within the configurations under consideration. We utilized in-house numerical codes developed with the OpenFOAM toolbox [24], an open-source library for computational fluid dynamics. Heat transfer in the geothermal heat exchanger and the surrounding soil was modeled and the simulations considered the coupled, conjugate transient heat transfer between each zone.

3.2.1. Governing equations

The problem under consideration involves an axisymmetric transient heat transfer in a laminar or turbulent developing flow of a Newtonian and incompressible fluid with constant properties.
The governing equations are solved through OpenFOAM C++ codes. They are expressed as follows:

- For the fluid:

Continuity equation:

$$\nabla \cdot \overrightarrow{v_f} = 0 \quad (31)$$

Where $\overrightarrow{v_f}$ is the fluid velocity.
Momentum equation:

$$\rho_f \frac{\partial \overrightarrow{v_f}}{\partial t} + \rho_f \nabla \cdot \left(\overrightarrow{v_f}\overrightarrow{v_f}\right) = -\nabla P + \nabla^2 \overrightarrow{v_f} \quad (32)$$

Where ρ_f is the fluid density and P the pressure.
Energy Equation:

$$\rho_f \frac{\partial E}{\partial t} + \nabla \cdot \left(\overrightarrow{v_f}\left(\rho_f E + P\right)\right) = \nabla \cdot \left(\lambda^* \nabla T_f\right) \quad (33)$$

Where:

$$E = h_{en} - \frac{P}{\rho_f} + \frac{{v_f}^2}{2} \quad (34)$$

$$h_{en} = \int_{T_{fref}}^{T_f} c_p dT_f + \frac{P}{\rho_f} \text{ (h_{en} is the enthalpy)} \quad (35)$$

$\lambda^* = \lambda_f + \lambda_t$ where λ_t represents the turbulent thermal conductivity.
For the turbulent case, two additional closure equations based on the $k-\epsilon$ realizable turbulence model were employed to calculate turbulent properties. A turbulent boundary layer based on y+ was utilized for near-wall treatment.

- For the solid (soil and tube):

Energy Equation:

$$\rho_s c_s \frac{\partial T_s}{\partial t} = \nabla \cdot (\lambda_s \nabla T_s) \quad (36)$$

3.2.2. Boundary and initial conditions

With reference to section 3.1, the boundary conditions applied are illustrated in Figure 3:

- Inlet: A boundary condition with uniform velocity $v_f = v_{f,in}$ and temperature $T_f(t) = T_f(0,t)$. In cases with turbulent flow, a turbulence intensity of 5% and the hydraulic diameter are specified.
- Outlet: The outlet is set as pressure outlet with $P_{out} = 0$.
- Outer soil: A constant temperature boundary condition with $T_s(r = r_e + D_s) = T_i$.
- Wedge/axisymmetric: Axisymmetric faces where the circumferential derivatives of flow variables are zero.

There are three regions (1 fluid and 2 solid) with a fluid-solid interface and a solid-solid interface. No-slip and no-penetration boundary conditions were imposed with energy flux conservation. Initially, all three computational domains are set to T_i, and the fluid region is initialized using the resolved steady-state solution for flow/turbulence fields.

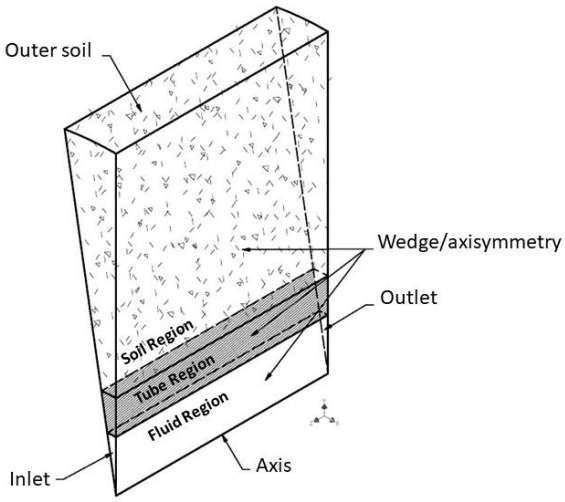

Figure 3. Regions and boundary conditions

3.2.3. Simulation approach

For each case, numerical simulations are conducted to evaluate heat transfer quantities for a duration of 10 days. Due to the long simulation time, various tests are performed to optimize computational efficiency. The computational regions are meshed using hexahedral blocks, and mesh sensitivity tests are conducted to determine the optimal mesh size, with adaptive time stepping. OpenFOAM is used to solve the governing equations in the computational domains for each set of boundary conditions. The simulation procedure is as follows (see figure 4):

First, the solution for laminar (or turbulent) flow is calculated in a steady-state condition, where only the flow/turbulence equations are solved until a converged flow-field solution is obtained. In this problem, the flow and heat transfer are decoupled since the thermo-physical properties are constant (no temperature-dependent properties or buoyancy forces). Therefore, the obtained velocity field is not time-dependent, so it is kept fixed for the transient heat transfer simulation. In the transient simulation, the flow field and turbulence are frozen, and the time-dependent temperature is specified at the inlet. The governing equations are iteratively solved using the finite-volume formulation with the PIMPLE algorithm (The PIMPLE Algorithm is a combination of PISO (Pressure Implicit with Splitting of Operator) and SIMPLE (Semi-Implicit Method for Pressure-Linked Equations)) [29], and convergence is determined by monitoring residuals and key integrated quantities.

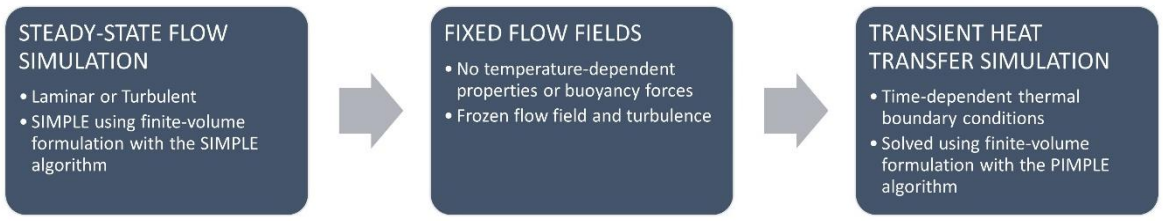

Figure 4. Simulation process

3.2.4. Data reduction

The physical quantities for fluid flow and heat transfer are calculated from the numerical velocity and temperature fields for each time step using the following definitions:

Fluid mean axial velocity is the integrated average axial velocity with respect to the flow area A_c:

$$v_{fm} = \frac{1}{A_c}\int_{A_c} v_f dA_c = \frac{\dot{m}}{\rho \cdot A_c} \quad (37)$$

The peripheral mean tube temperature $T_t(t,z,r_i)$, fluid bulk mean temperature $T_f(t,z)$ and-peripheral mean tube heat flux $\varphi_t(t,z,r_i)$ at an arbitrary cross section in z are respectively calculated using:

$$T_t(t,z,r_i) = \frac{1}{pe}\int_{pe} T_f dpe \quad \text{where } pe \text{ is the inside perimeter of the tube.} \quad (38)$$

$$T_f(t,z) = \frac{1}{A_c\, v_{fm}}\int_{A_c} v_f\, T_f dA_c \quad (39)$$

$$\varphi_t(t,z,r_i) = \frac{1}{pe}\int_{pe} \varphi_t\, dpe \qquad \text{where } \varphi_t \text{ is the flux density on the tube inner wall} \quad (40)$$

3.2.5. Numerical Results

For the flow field, the numerical simulation results are compared with available literature data for the steady flow field. Analytical solutions and correlations exist for the velocity profile of hydrodynamically developed laminar flow [25], and turbulent flow regime [26], in the latter case, the 1/7th power law an analytical and empirical formulation of the turbulent velocity profile. Figure 5 shows a good agreement between the analytical and simulated velocity profiles in the laminar and turbulent regimes for both water and air.

a) b)

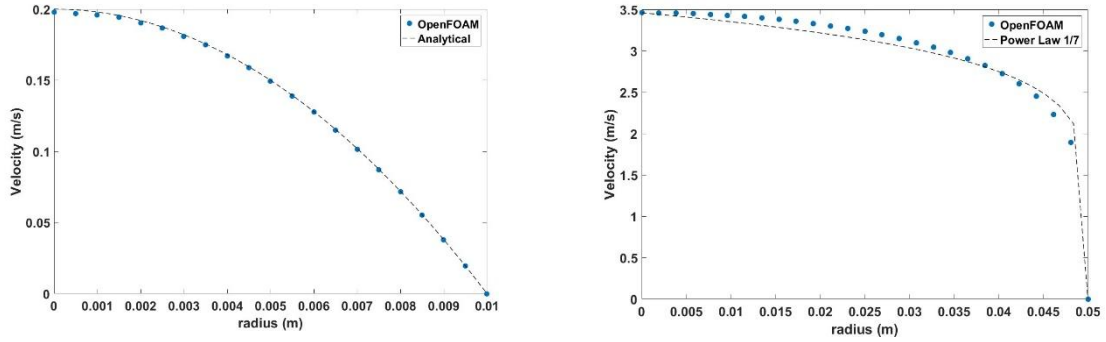

Figure 5. a) Radial water velocity profile for $v_f = 0.1\ m/s$ (laminar flow); b) Radial air velocity profile for $v_f = 2.829\ m/s$ (turbulent flow)

In the next section, and for all case, the analytical model will be compared to the numerical results. It is worth noting that all numerical computation took 40 hours using a 6 cores Ubuntu machine each with max frequency of 4800 MHz.

3.3. Quadrupole analytical model validation

The aim of this section is to compare the analytical model with the complete numerical solution (2D axisymmetric) for the several cases described in Table 2. Two approaches are considered, one where the convective heat transfer coefficient in R_f is estimated using the following empirical correlation [27]:

- Laminar flow:

  $$Nu = 4.36 \quad (41)$$

- Turbulent flow:

$$Nu = 0.023\, Re^{0.8}\, Pr^{1/3} \quad (42)$$

The second approach is where the fluid convective heat transfer coefficient is identified from the numerical results using curve fitting.

3.3.1. Air ground-coupled heat exchanger

This sub-section considers cases 1, 2, 7, and 8 where the working fluid is air. For these cases, the analytical model is used to predict the air outlet temperature considering the following values of the parameters:

- Buried pipe: length 20 m, internal radius 5 cm, wall thickness 2 mm.
- Initial soil temperature: $T_i = 0°C$
- Constant fluid inlet temperature (cases 1 and 2): $T_f(0) = 20°C$
- Periodic fluid inlet temperature (cases 7 and 8): $T_f(0,t) = T_{f0}\cos(\omega t)$ with $T_{f0} = 20°C$; $\omega = \frac{2\pi}{24\times3600}$
- Convective heat transfer coefficient calculated through relation (42): $h = 13.6\ \mathrm{W\ m^{-2}\ K^{-1}}$

Figure 6 shows the heat exchanger outlet temperatures obtained for cases 1 and 2 (constant inlet temperatures). Each figure features 2 curves, the temperature calculated with OpenFOAM and the temperature calculated using the quadrupole analytical model. Figure 7 shows the air outlet temperature obtained for case 7 and case 8.

a) b)

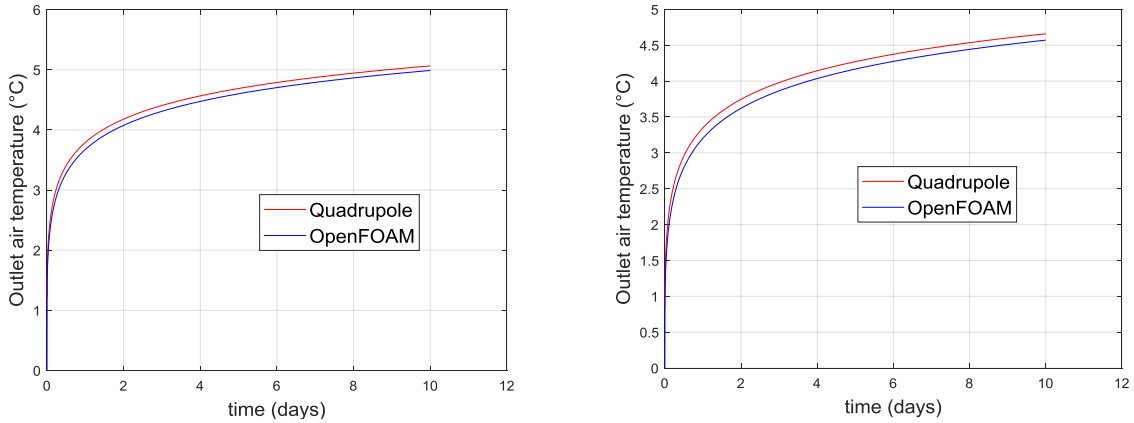

Figure 6. Outlet Air temperature in a) Case 1; b) Case 2

a) b)

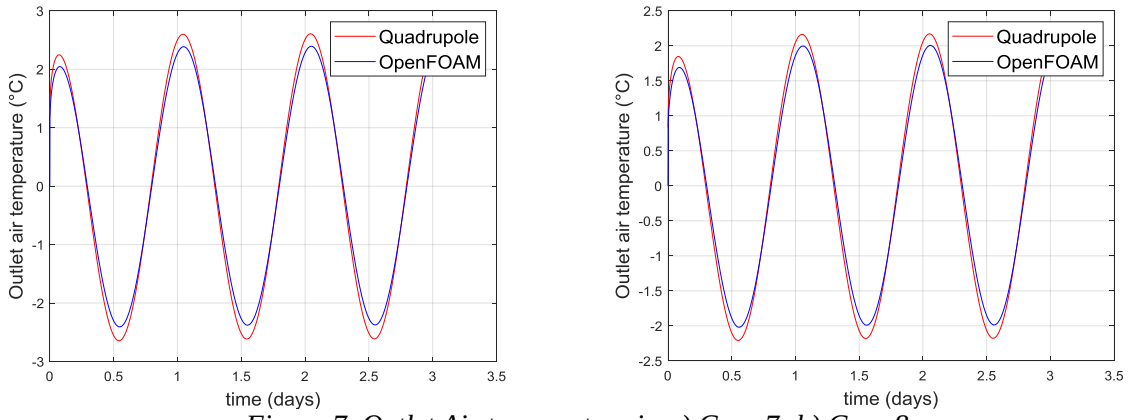

Figure 7. Outlet Air temperature in a) Case 7; b) Case 8

The agreement between the numerical and analytical results is very good, with a temperature difference of less than 0.2°C between the two. Moreover, if we identify the fluid convective exchange coefficient from the numerical result, the 2 curves overlap perfectly, as can be seen for example in Figure 8 for Case 1, having $h = 13.9\ \mathrm{W\,m^{-2}\,K^{-1}}$ (instead of the calculated 13.6 $\mathrm{W\,m^{-2}\,K^{-1}}$). Bearing in mind that correlations only provide orders of magnitude, therefore the results obtained validate the analytical approach for air-ground heat exchanger.

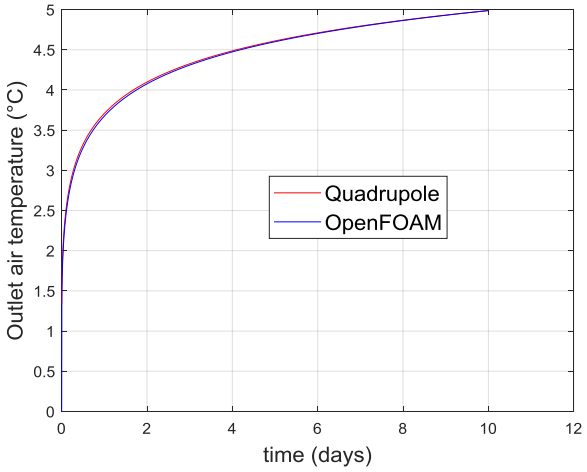

Figure 8. Outlet Air temperature with identified h

3.3.2. Water ground-coupled heat exchanger

The same validation steps will be used for the remaining cases 3, 4, 5, 6, 9, and 10 where the working fluid is water. The analytical model parameters are:

- Buried pipe: length 30 m, internal radius 1 cm, wall thickness 2 mm.
- Initial soil temperature: $T_i = 0°\mathrm{C}$
- Constant fluid inlet temperature (cases 3, 4, 5, and 6): $T_f(0) = 20°\mathrm{C}$
- Periodic fluid inlet temperature (cases 9 and 10): $T_f(0,t) = T_{f0}\cos(\omega t)$ with $T_{f0} = 20°\mathrm{C}$; $\omega = \frac{2\pi}{24\times3600}$
- The calculated laminar convective heat transfer coefficient through relation (41) $h = 131\ \mathrm{W\,m^{-2}\,K^{-1}}$.
- The calculated turbulent convective heat transfer coefficient through relation (42) $h = 3620\ \mathrm{W\,m^{-2}\,K^{-1}}$

Figure 9 show the outlet water temperatures for cases 3 to 6 with constant inlet temperature. Figure 10 show the outlet water temperatures for cases 9 and 10 with periodic inlet temperature. Each plot features 2 curves, the temperature calculated with OpenFOAM and the one calculated with the analytical model. The differences are even smaller than for the air geothermal heat exchanger. In fact, the higher the exchange coefficient, the closer the two models are.

a) b)

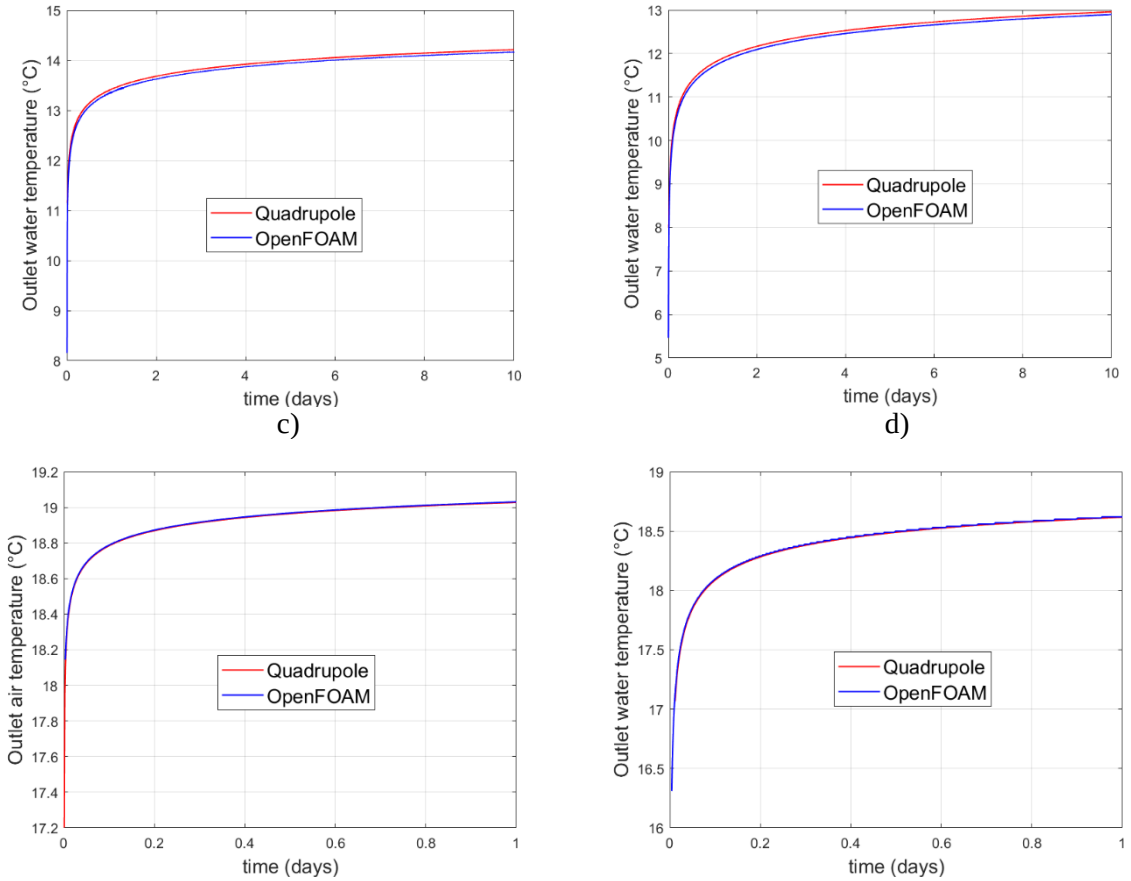

Figure 9. Outlet water temperature in a) Case 3; b) Case 5; c) Case 4; d) Case 6

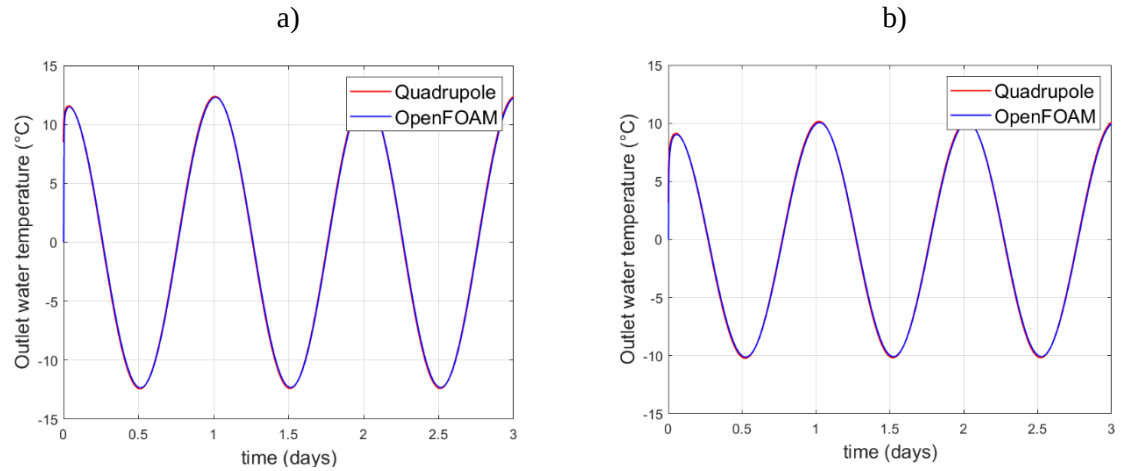

Figure 10. Outlet water temperature in a) Case 9; b) Case 10

4. Comparison with some analytical models in the literature:

In this section, the analysis is extended by comparing the proposed model to four existing analytical models available in the literature. These reference models employ distinct approaches to simulate heat transfer between the fluid and the ground. By examining a range of cases, the performance of the model is systematically evaluated against these conventional models. As brief description of the models now follows.

4.1. Model 1: The ground is at constant temperature

This model considers the following assumptions [28, 29]:

- Ground temperature is uniform and constant.
- Tube temperature is uniform and equal to ground temperature (low tube thickness and low convection coefficient).
- The heat balance in the tube is applied locally.

The temperature at distance L from the tube inlet is therefore given by:

$$T_f(L) = T_i + \left[T_f(0) - T_i\right] exp\left(-\frac{2\pi h r_i L}{\dot{m}_f c_f}\right) \quad (43)$$

Where $\dot{m}_f = \rho_f v_f A$ is the mass flow rate and h is the convection transfer coefficient between the fluid and the tube.

4.2. Model 2: The ground is a thermal resistance

This model considers the following assumptions [30, 31]:

- Soil temperature is uniform and constant at a distance δ from the tube.
- Thermal inertia of the ground is neglected.
- Tube temperature is uniform.
- The balance in the tube is applied locally.

The temperature at distance L from the tube inlet is therefore given by:

$$T_f(L) = T_i + \left[T_f(0) - T_i\right] exp\left(-\frac{2\pi U r_i L}{\dot{m}_f c_f}\right) \quad (44)$$

Where:

$$U = \frac{1}{2\pi r_i L}\ \frac{1}{R_f + R_t + R_s} \quad (45)$$

$$R_s = \frac{ln\left(\frac{r_e+\delta}{r_e}\right)}{2\pi\lambda_s L} \quad (46)$$

R_f and R_t are given by relations (8) and (9).

with $r_e = r_i + e$; $\lambda_s = 1.9$ W m^{-1} K^{-1} ; $\rho_s c_s = 1.9 \times 10^6$ W m^{-3} K^{-1}. δ is the depth of penetration into the ground of the heat flux produced by a daily period excitation of the tube, according to [30], $\delta = 0.17\ m$ for a period of one day and $\delta = 3\ m$ for a period of one year.

4.3. Model 3: Ground resistance variable with time, global heat balance

This model considers the following assumptions [2, 8]:

- Ground resistance is modeled by the infinite source line model.
- Tube temperature is uniform.
- The balance in the tube is applied globally.

Based on equations provided in [3], we have:

$$G(t) = E_1\left(\frac{r_e^2}{4a_s t}\right)/(4\ pi\ \lambda_s) \quad (47)$$

$G(t)$ is the transient part of the thermal resistance and E_1 the exponential integral:

$$E_1\left(\frac{r_e^2}{4a_s t}\right) = \int_{\frac{r_e^2}{4a_s t}}^{\infty} \frac{\exp(-u)}{u} du \quad (48)$$

The resistance per unit length is:

$$R(t) = (R_f + R_t)\, L + G(t) \quad (49)$$

The overall heat balance on the tube:

$$\dot{m}_f c_f \big(T_f(0) - T_f(L)\big) = q\, L \quad (50)$$

With $T_f(0)$ and $T_f(L)$ the temperatures at the inlet and outlet of the tube respectively. The heat exchange between the tube and the ground is:

$$q = \frac{T_f - T_i}{R(t)} \quad (51)$$

With T_f the fluid average temperature $T_f = \big(T_f(0) - T_f(L)\big)/2$. Using equations (49), (50), and (51), we obtain the temperature at distance L from the tube's inlet:

$$T_f(L) = T_f(0)(1+K)/(1-K) - T_i\, 2\, K/(1-K) \quad (52)$$

Where: $K = L/(2\dot{m}_f c_f\, R(t))$ (53)

4.4. Model 4: Ground resistance varies with time, local heat balance

This model corresponds to model 2, in which the constant ground resistance is replaced by the variable resistance of model 3. The assumptions are:

- Ground resistance is modeled by the infinite source line model.
- Tube temperature is uniform.
- The balance in the tube is applied locally.

The temperature at distance L from the tube's inlet:

$$T_f(L) = T_i + \big[T_f(0) - T_i\big]\, exp\left(-\frac{2\pi U r_i L}{\dot{m}_f c_f}\right) \quad (54)$$

Where: $U = \frac{1}{2\pi r_i L}\ \frac{1}{R_f + R_t + G(t)/L}$ (55)

4.5. Analytical models' comparison

The proposed analytical model "quadrupole" is compared to the four preceding models for the cases described in table 4.

Table 4. Analytical models' comparisons cases

Case N°	Inlet temperature $T_f(0)$	Initial temperature T_i	Fluid type	Tube material	$v_f(m/s)$
11	Constant 0°C	12°C	Air	PVC	2.83
12	Constant 30°C	12°C	Air	PVC	2.83
13	Constant 0°C	12°C	Water	PVC	0.1
14	Constant 30°C	12°C	Water	PVC	0.1
15	Variable 0°C to 30°C	12°C	Air	PVC	2.83
16	Variable 0°C to 30°C	12°C	Water	PVC	0.1

Figures 11 and 12 show the results of the five models for the different cases. In the case of water ground-coupled heat exchanger, i.e., with a high fluid convective heat exchange coefficient, apart from

the elementary models 1 and 2, the 3 other models give similar results (Figure 11.c, Figure 11.d, and Figure 12.b). On the other hand, for air ground-coupled heat exchanger (low convective heat exchange coefficient), all the models presented in the literature deviate from our model, validated by a numerical calculation without approximation (figure 12.a). It is interesting to note that Model 4 gives identical results to our model when the inlet fluid temperature is constant (Figure 11.a and Figure 11.b). In fact, in model 4, the convolution product has been approximated by a simple product, which is correct if one of the 2 terms of the product is a constant (for case 15, figure 12.a, model 4 is no longer satisfactory).

a) Air

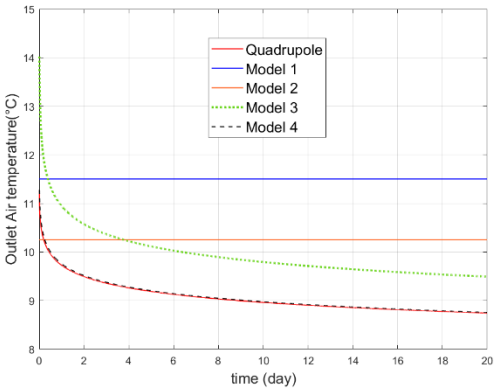

b) Air

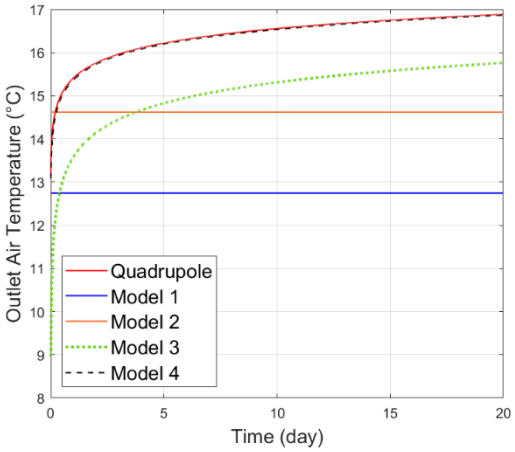

c) Water

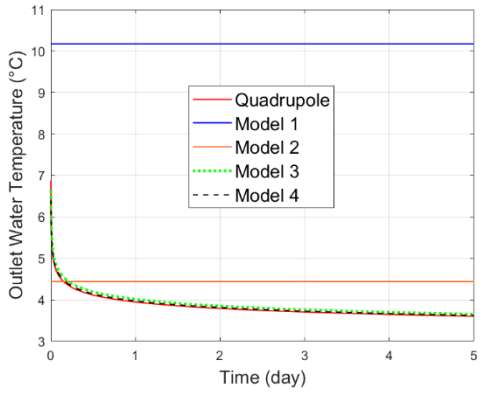

d) Water

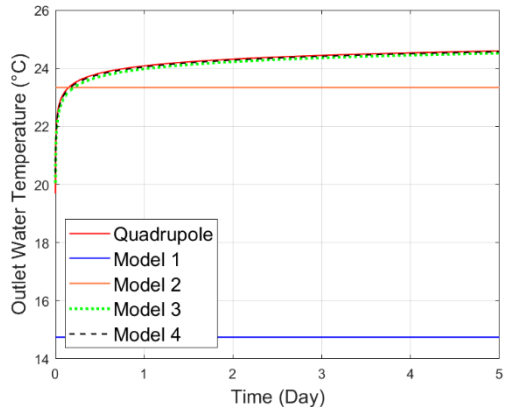

Figure 11. Outlet temperature for a) Case 11; b) Case 12; c) Case 13; d) Case 14

a) Air

b) Water

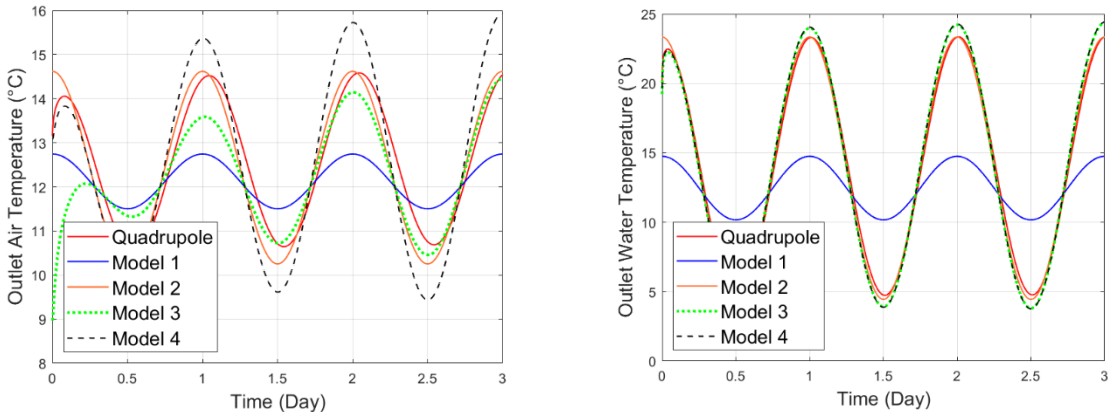

Figure 12. Outlet temperature for a) Case 15; b) Case 16

Conclusion

The aim of this study is to propose a new analytical model for the prediction of the transient thermal performance of single tube geothermal heat exchanger. The proposed model is validated for different cases with different geometrical, flow, and thermal conditions against numerical simulations using OpenFOAM. The proposed model is then compared to four analytical model available in the literature covering different approach to ground modeling. The following conclusion are drawn:

- Prediction based on analytical heat-transfer models is the most practical and cost-efficient approach to modeling ground heat exchangers compared to numerical simulations. In the present work, numerical simulations took a total of 40h while all analytical calculation with the proposed model took less than 5 min with less than 0.1 K of difference.
- Elementary ground models cannot make sufficiently accurate transient temperature predictions.
- Models based on the infinite line source model can provide appropriate temperature predictions for cases with high convective heat transfer coefficient, but with limited accuracy where the fluid convective heat transfer is low.
- The proposed "quadrupole" analytical model is more accurate as it can predict the thermal performance without the limitations on heat and flow conditions.

References:

1. Khaleghi, K., & Livescu, S. (2023). A review of vertical closed-loop geothermal heating and cooling systems with an Emphasis on the importance of the subsurface. *Journal of Petroleum Science and Engineering*, *220*, 111137.
2. Li, M., & Lai, A. C. (2015). Review of analytical models for heat transfer by vertical ground heat exchangers (GHEs): A perspective of time and space scales. *Applied Energy*, *151*, 178-191.
3. Yang, H., Cui, P., & Fang, Z. (2010). Vertical-borehole ground-coupled heat pumps: A review of models and systems. *Applied energy*, *87*(1), 16-27.
4. Chen, Y., Pan, B., Zhang, X., & Du, C. (2019). Thermal response factors for fast parameterized design and long-term performance simulation of vertical GCHP systems. *Renewable Energy*, *136*, 793-804.
5. Cui, Y., Zhu, J., Twaha, S., & Riffat, S. (2018). A comprehensive review on 2D and 3D models of vertical ground heat exchangers. Renewable and sustainable energy reviews, 94, 84-114.
6. Pei, L., Schalbart, P., & Peuportier, B. (2022). A global model for fast calculation of the thermal response factor of large-scale boreholes heat exchangers combining the FLS model, the 2D heat equation and a three-points method. *Energy and Buildings*, *276*, 112536.

7. Spitler, J. D., & Gehlin, S. E. (2015). Thermal response testing for ground source heat pump systems—An historical review. Renewable and Sustainable Energy Reviews, 50, 1125-1137.
8. Carslaw, H. S., Jaeger, J. C., & Feshbach, H. (1962). Conduction of heat in solids. *Physics Today*, *15*(11), 74-76.
9. Ingersoll, L. R., Zobel, O. J., & Ingersoll, A. C. (1954). Heat conduction: With engineering, geological, and other applications. Madison: University of Wisconsin Press.
10. Zeng, H. Y., Diao, N. R., & Fang, Z. H. (2002). A finite line- source model for boreholes in geothermal heat exchangers. Heat Transfer—Asian Research: Co- sponsored by the Society of Chemical Engineers of Japan and the Heat Transfer Division of ASME, 31(7), 558-567.
11. Yang, Y., & Li, M. (2014). Short-time performance of composite-medium line-source model for predicting responses of ground heat exchangers with single U-shaped tube. International Journal of Thermal Sciences, 82, 130-137.
12. Choi, W., & Ooka, R. (2016). Effect of disturbance on thermal response test, part 2: Numerical study of applicability and limitation of infinite line source model for interpretation under disturbance from outdoor environment. Renewable Energy, 85, 1090-1105.
13. Choi, W., & Ooka, R. (2015). Interpretation of disturbed data in thermal response tests using the infinite line source model and numerical parameter estimation method. Applied Energy, 148, 476-488.
14. Pasquier, P., & Lamarche, L. (2022). Analytic expressions for the moving infinite line source model. Geothermics, 103, 102413.
15. Lee, C. K. (2011). Effects of multiple ground layers on thermal response test analysis and ground-source heat pump simulation. Applied Energy, 88(12), 4405-4410.
16. Mottaghy, D., & Dijkshoorn, L. (2012). Implementing an effective finite difference formulation for borehole heat exchangers into a heat and mass transport code. Renewable energy, 45, 59-71.
17. Harris, B. E., Lightstone, M. F., Reitsma, S., & Cotton, J. S. (2022). Analysis of the transient performance of coaxial and u-tube borehole heat exchangers. Geothermics, 101, 102319.
18. Gustafsson, A. M., Westerlund, L., & Hellström, G. (2010). CFD-modelling of natural convection in a groundwater-filled borehole heat exchanger. Applied thermal engineering, 30(6-7), 683-691.
19. Pasquier, P., & Marcotte, D. (2014). Joint use of quasi-3D response model and spectral method to simulate borehole heat exchanger. Geothermics, 51, 281-299.
20. Formhals, J., Welsch, B., Hemmatabady, H., Schulte, D. O., Seib, L., & Sass, I. (2022). Co-simulation of district heating systems and borehole heat exchanger arrays using 3D finite element method subsurface models. Journal of Building Performance Simulation, 15(3), 362-378.
21. Pei, L., Schalbart, P., & Peuportier, B. (2022). A global model for fast calculation of the thermal response factor of large-scale boreholes heat exchangers combining the FLS model, the 2D heat equation and a three-points method. Energy and Buildings, 276, 112536
22. Ahmed, S. F., Liu, G., Mofijur, M., Azad, A. K., Hazrat, M. A., & Chu, Y. M. (2021). Physical and hybrid modelling techniques for earth-air heat exchangers in reducing building energy consumption: Performance, applications, progress, and challenges. *Solar Energy*, *216*, 274-294.
23. Den Iseger P.(2006). Numerical Transform Inversion using Gauss Quadrature. Probability in theEngin. and Inform. Sci., 20, 1-44.
24. H. G. Weller, G. Tabor, H. Jasak, C. Fureby, A tensorial approach to computational continuum mechanics using object-oriented techniques, COMPUTERS IN PHYSICS, VOL. 12, NO. 6, NOV/DEC 1998.
25. White, F. M. (1990). Fluid mechanics. New York.
26. De Chant, L.
27. J. (2005). The venerable 1/7th power law turbulent velocity profile: a classical nonlinear boundary value problem solution and its relationship to stochastic processes. Applied Mathematics and Computation, 161(2), 463-474.
28. Incropera, F. P., DeWitt, D. P., Bergman, T. L., & Lavine, A. S. (1996). Fundamentals of heat and mass transfer (Vol. 6, p. 116). New York: Wiley.

29. Bisoniya, T. S. (2015). Design of earth–air heat exchanger system. *Geothermal Energy*, *3*, 1-10.
30. Li, Z. X., Shahsavar, A., Al-Rashed, A. A., Kalbasi, R., Afrand, M., & Talebizadehsardari, P. (2019). Multi-objective energy and exergy optimization of different configurations of hybrid earth-air heat exchanger and building integrated photovoltaic/thermal system. *Energy Conversion and Management*, *195*, 1098-1110.
31. Hollmuller, P., & Lachal, B. (2014). Air–soil heat exchangers for heating and cooling of buildings: Design guidelines, potentials and constraints, system integration and global energy balance. *Applied Energy*, *119*, 476-487.
32. Amanowicz, Ł., & Wojtkowiak, J. (2021). Comparison of single-and multipipe earth-to-air heat exchangers in terms of energy gains and electricity consumption: A case study for the temperate climate of central europe. *Energies*, *14*(24), 8217.
33. "Greenshields, C. J., & Weller, H. G. (2022). Notes on computational fluid dynamics: General principles."

Appendix 1:

Figure A.1 present the radial velocity profile for water in turbulent flow conditions.

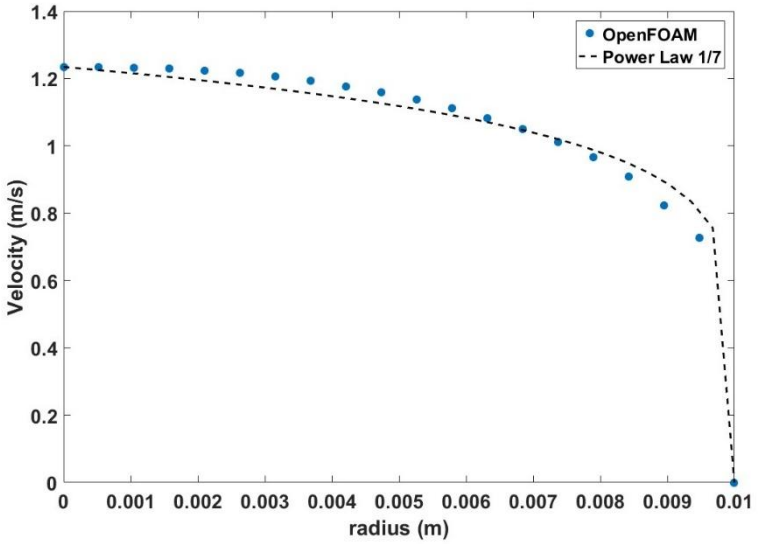

Figure A.1: Radial water velocity profile for $v_f = 1\ m/s$ (turbulent flow)